Atomistic simulations of spin-lattice coupling effects on magnetomechanics in skyrmion materials

Yifeng Wu,[1] Haohua Wen,[1,*] Jianyi Liu,[1] Kan Lai,[1] and Yue Zheng[1,2,†]

[1]*Micro&Nano Physics and Mechanics Research Laboratory, School of Physics, Sun Yat-sen University, Guangzhou 510275, China*

[2]*State Key Laboratory of Optoelectronic Materials and Technologies, School of Physics, Sun Yat-sen University, Guangzhou 510275, China*

(Received 14 August 2019; revised manuscript received 9 September 2019; published 31 October 2019)

Skyrmion-based spintronic devices are considered one of the prime candidates for the next generation of functional devices. The mechanistic understanding of magnetomechanics arising from the intrinsic spin-lattice coupling in skyrmion materials becomes an attractive issue. In this paper, by taking MnSi as an example, we proposed an atomistic simulation model based on the developed spin-lattice dynamics scheme for skyrmion materials. The calculated magnetomechanical properties are examined to be qualitatively consistent with the experimental measurement, which suggests that our model is appropriate for the study of thermodynamics, magnetics, and mechanics of skyrmion materials. In addition, the microscopic understanding of the thermodynamic and kinetic aspects of magnetomechanics in skyrmion materials are presented. Through the intrinsic spin-lattice coupling, the transformation of magnetic ordering by external magnetic field results in the change of mechanical properties, for instance, the global mechanical anisotropy and local distortion of lattice structure. The calculation results indicate the magnetomechanics are the result of spin nonalignment induced by the synergistic effects of Dzyaloshinsky-Moriya interaction, Heisenberg exchange interaction, and Zeeman interaction of interspins and elastic interactions of interlattices. Further, the relaxation time of the lattice structure is calculated to characterize the speed of mechanical response against the magnetic ordering changes, which might provide hints of low-energy consumption and low applied electric current in driving skyrmions. The microscopic understanding provided by current study could help the research and design of skyrmion-based spintronic devices.

DOI: 10.1103/PhysRevB.100.144310

I. INTRODUCTION

Magnetic skyrmions (skyrmions for short in the rest of paper), a kind of topologically protected chiral swirling spin texture, have been found in various materials with broken inversion symmetry, owing to the intrinsic spin-orbit coupling and described by the so-called Dzyaloshinsky-Moriya interaction (DMI) [1,2], which makes the nonalignment of atomic spins against the action of Heisenberg exchange interaction (HEI) under certain external environments. Compared to the traditional ferromagnetic domain structure, skyrmions have many excellent physical properties, such as nanoscale size [3], topological stability [4], sensitive manipulation by magnetic [5,6], mechanical [7,8], or electrical loading [9,10] with low-energy consumption [11]. Therefore, skyrmion-based devices are considered one of the prime candidates for the next generation of spintronic functional devices [12]. Starting in 2009, studies have been performed on the issues of skyrmions related to materials engineering [13–18], fundamental manipulation approaches [5–10], and device designs [12], etc.. For the issue of skyrmion manipulation, substantial progress has been made, such as modulation by electric current [19,20], magnetic field [5,6], stress [7,8], and temperature gradient [21,22]. Recently, the skyrmion structure was found to be sensitive to its mechanical environment [14], which promotes skyrmion-based devices as a prime candidate for magnetic-mechanical sensors [23]. There are twofold aims in this paper: (1) Taking the typical B20-type MnSi as an example, we construct an atomic-based spin-lattice dynamics (SLD) scheme for the study of thermodynamics of skyrmion-materials [24] and (2) by performing atomic simulations, we aim to study the physical picture of the magnetomechanical phenomena in skyrmion materials, which is considered a significant issue in the field of skyrmion-based spintronics [25].

Studies of magnetic-mechanical phenomena in magnetic materials could be traced back to Joule's magnetostriction effect [26], which is induced by the magnetic anisotropic interaction due to spin-orbit coupling effects. Kittel [27] proposed a magnetomechanical theory in 1949 by introducing an empirical term on the basis of Landau-type free-energy expression to describe the magnetostriction effects. In 1982, Plumer *et al.* [28,29] promoted this empirical theory to chiral magnetic materials and found the anomalous magnetic-induced elastic responses in B20-type MnSi, that there is an abrupt change in elastic moduli across the phase boundary between ferromagnetic and spiral magnetic ordering phases, and that it has been confirmed by ultrasound measurement [30] in 2009. Recently, the phenomenological theoretical models are being further improved, based on which increasingly sophisticated magnetic-mechanical phenomena in skyrmion materials have been revealed [31–34]. On the other hand, due to the great success of the so-called micromagnetic modeling scheme (based on Landau-Lifshitz-Gilbert (LLG) equation [35]) on studying the thermodynamic and kinetic behaviors in the traditional

*Corresponding author: wenhh3@mail.sysu.edu.cn
†Corresponding author: zhengy35@mail.sysu.edu.cn

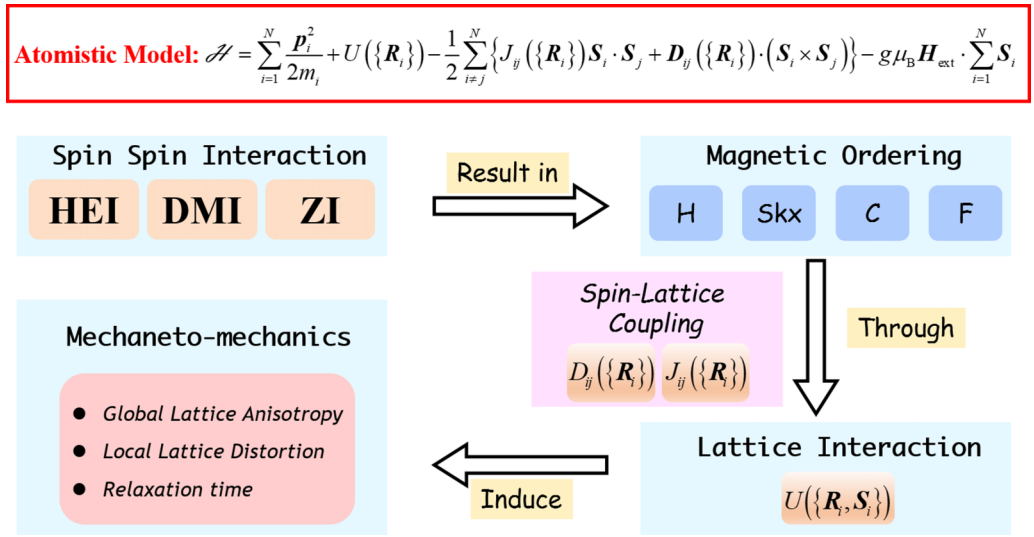

FIG. 1. The physical mechanism of magnetomechanics. The atomistic spin-lattice coupling system is described by the Hamiltonian at the top of figure. The spin-spin interactions [including Heisenberg exchange interaction (HEI), Dzyaloshinsky-Moriya interaction (DMI), and Zeeman interaction (ZI)] results in four magnetic ordering phases [helical (H), skyrmion crystal (Skx), conical (C), and ferromagnetic (F)], respectively. Through the intrinsic spin-lattice coupling described by $J_{ij}(\boldsymbol{R})$ and $\boldsymbol{D}_{ij}(\boldsymbol{R})$, the magnetic ordering brings the extra contribution to the lattice interactions, and thus results in the magnetomechanics.

magnetic materials, the corresponding microscopic modeling scheme for skyrmion materials was recently developed by introducing the similar magneto-mechanical coupling effects into the LLG equations, where the microscopic DMI term is used to represent the actions of spin-orbit coupling. Note that, in the models mentioned above, the magnetic and mechanical interactions in skyrmion materials are adiabatically separated and their coupling is treated as a perturbation with an empirical magneto-mechanical tensor to describe the coupling strength [27,28]. Therefore, it is not clearly clarified on the mechanistic understanding on the physical origination of the introduced phenomenological magnetic-mechanical coupling term, which requires an atomistic physical picture bridging from the actions of spin-orbit coupling on the electronic level to the phenomenological magnetic-mechanical coupling on macroscopic level.

In the point of view of atomic scale, the motions of atomic spins (spin for short in the rest of the paper) and atomic lattice (lattice for short in the rest of the paper) in magnetic materials are instantaneously coupled together, which is so-called spin-lattice coupling [36]. Here, the magnetism is characterized by spins, and the strength of magnetic interaction is determined by the wave-function overlapping of the neighboring spins, which relies on the atomic distance and the local environment [37]. In particular, the vibrations of lattices at finite temperatures, i.e., phonon, result in the instantaneous change of spin-spin interactions strength, giving rise to the magnetic ordering modulation. On the other hand, the vibrations of spins, resulting in the low-lying thermal excitation, i.e., magnon, would also vary lattice-lattice interactions, giving rise to magnetic-induced mechanical properties. The latter is indeed the atomistic physical picture of the magnetostriction effects induced by spin-lattice coupling. Note that, when the vibrational frequencies of magnon modes are not comparable with those of phonons, their coupling is sufficiently weak to ensure the adiabatic treatment of the mechanical and magnetic interactions is appropriate and the coupling effects could be well described as a perturbation in the above-mentioned theoretical models [27,28]. However, near magnetic phase boundaries, the softening of magnon modes induced by phase transition might lead to the strong anharmonic interactions with phonon modes [38], giving rise to the magnetic anomalous phenomena, e.g., the so-called magnetic diffusion anomaly in ferromagnetic iron [39], which is not appropriate to be described by the perturbation theory mentioned above [27,28]. In addition, the magnetic and mechanical responses in skyrmion materials are indeed of dynamical processes, with respect to the relaxation of phonon and magnon modes, as well as their interactions, which is beyond the capability of the phenomenological theoretical models. In this regard, the atomistic modeling is required to get a clear physical picture of the magnetostriction effects. The developed SLD [36] provides a practical tool for studying the magnetic anomaly, where the vibrations of spins and lattices are treated instantaneously, and the spin-lattice coupling is determined by a lattice-configuration-dependent Heisenberg-type spin-spin exchange interaction function.

In this paper, on the basis of the SLD framework for magnetic materials, we propose an atomistic description for magnetomechanics of skyrmion materials, taking MnSi as an example. Using the modified SLD model, as shown in Fig. 1, the spin-lattice coupled system is described by the atomistic model and the bottom-up idea of research is shown from the left to right in Fig. 1. Due to the spin-spin interactions, including HEI, DMI, and ZI, four magnetic ordering structures appear with the increase of the applied external magnetic field ($\boldsymbol{H}_{\mathrm{ext}}$), i.e., helical (H), skyrmion crystal (Skx), conical (C), and ferromagnetic (F) phases. Because of the intrinsic spin-lattice coupling [described by $J_{ij}(\{\boldsymbol{R}_i\})$ and $\boldsymbol{D}_{ij}(\{\boldsymbol{R}_i\})$ in the current atomic model], the spin-spin arrangement can modulate the lattice configuration. In

addition, the lattice-lattice interaction $\boldsymbol{U}(\{\boldsymbol{R}_i\})$ would resist this modulation. Hence, the magneto-mechanical properties should be the result of the synergistic effects of HEI, DMI, the ZI, and lattice-lattice interaction. In the current paper, the mechanical responses due to magnetic ordering transition are represented by global lattice anisotropy (i.e., magnetostriction) and local distortion, revealing the thermodynamics of the system with spin-lattice coupling, which gives hints for the research and design of the magneto-mechanical sensors or multiferroic devices. Further, the energetic consumption and modulation speed are important considerations in the materials engineering; therefore, the characteristic time of mechanical response is also studied in this paper, which is represented by the characteristic relaxation time of lattice structure changes with the magnetic ordering phase transition, associated with the dynamical relaxations of phonon modes. We hope our results can provide a microscopic understanding of the spin-lattice coupling and the resulting magnetostriction effects, giving rise to an accurate prediction for manipulation of mechanical and magnetic properties in skyrmion materials. The paper is organized as follows: the brief introduction of theoretical model and simulation detail will be presented in Secs. II and III, respectively, following which the results and discussion are put in Sec. IV, and finally the conclusion is drawn in Sec. V.

II. ATOMISTIC SIMULATION MODEL

SLD is developed on the basis of the conventional molecular dynamics scheme to describe the thermodynamics of ferromagnetic materials [36] with a spin-lattice coupled Hamiltonian. Solving the resulting equations of motion for lattice and spin degrees of freedom under a specific external condition, the time-dependent phase-space trajectories are collected, from which the thermodynamic observations are calculated following statistical thermodynamic theories under the ergodicity hypothesis.

A. Hamiltonian and equations of motion

For the typical skyrmion material, e.g., MnSi, which has a noncentral symmetrical B20 crystal structure, the magnetism is originated from the Mn atoms [40]. In analog to ferromagnetic iron, we simplified such a system as an ensemble of interactive Heisenberg particles with the lattice and spin degrees of freedom involved, where each particle stands for a B20 unit cell containing Mn_3Si_3. In atomistic modeling, such an ensemble of Heisenberg particles is embedded in a noisy environment $\mathcal{H}_{\rm env}$ denoted by temperature T, whose Hamiltonian $\mathcal{H}$ could be written as [36]

$$\begin{aligned}\mathcal{H} = &\sum_i \frac{\boldsymbol{p}_i^2}{2m_i} + U(\{\boldsymbol{R}_i\}) \\ &-\frac{1}{2}\sum_{i\neq j}^{N}[J_{ij}(\{\boldsymbol{R}_i\})\boldsymbol{S}_i\cdot\boldsymbol{S}_j + \boldsymbol{D}_{ij}(\{\boldsymbol{R}_i\})\cdot(\boldsymbol{S}_i\times\boldsymbol{S}_j)] \\ &-g\mu_{\rm B}\boldsymbol{H}_{\rm ext}\sum_{i=1}^{N}\boldsymbol{S}_i + \mathcal{H}_{\rm env}. \end{aligned} \tag{1}$$

Here, m_i, $\boldsymbol{p}_i$, $\boldsymbol{R}_i$, and $\boldsymbol{S}_i$ are, respectively, the atomic mass, momentum, coordinate, and spin vector of the ith particle. $U(\boldsymbol{R})$ describes the nonmagnetic interactions of the lattice subsystem. The terms of $J_{ij}(\boldsymbol{R})\boldsymbol{S}_i\cdot\boldsymbol{S}_j$ and $\boldsymbol{D}_{ij}(\boldsymbol{R})\cdot(\boldsymbol{S}_i\times\boldsymbol{S}_j)$, respectively, represent the inter-spin HEI and DMI, whose interaction strengths, i.e., $J_{ij}(\boldsymbol{R})$ and $\boldsymbol{D}_{ij}(\boldsymbol{R})$, are the functions of lattice configuration $\boldsymbol{R}\equiv\{\boldsymbol{R}_i\}$. In particular, the term of $\boldsymbol{S}_i\times\boldsymbol{S}_j$ illustrates the exchange asymmetry between $\boldsymbol{S}_i$ and $\boldsymbol{S}_j$, which is also the source of chirality of the spiral spin texture. The third term on the right-hand side of Eq. (1) is the Zeeman term, with $\boldsymbol{H}_{\rm ext}$ the external magnetic field, $g\approx 2$ the spin g-factor, and $\mu_{\rm B}$ the Bohr magneton. From Eq. (1), the equations of motion for the spin and lattice degrees of freedom can be derived as

$$\begin{cases} \frac{\partial \boldsymbol{R}_i}{\partial t} = \frac{\boldsymbol{p}_i}{m} \\ \frac{\partial \boldsymbol{p}_i}{\partial t} = -\frac{\partial U}{\partial \boldsymbol{R}_i} + \sum_j\left[\frac{\partial J_{ij}}{\partial \boldsymbol{R}_i}(\boldsymbol{S}_i\cdot\boldsymbol{S}_j) + \frac{\partial \boldsymbol{D}_{ij}}{\partial \boldsymbol{R}_i}\cdot(\boldsymbol{S}_i\times\boldsymbol{S}_j)\right] \\ \qquad\qquad -\gamma_i^L\boldsymbol{p}_i + \boldsymbol{f}_i(t) \\ \hbar\frac{\partial \boldsymbol{S}_i}{\partial t} = \boldsymbol{S}_i\times[\boldsymbol{H}_i + \boldsymbol{h}_i(t)] - \gamma_i^S\boldsymbol{S}_i\times(\boldsymbol{S}_i\times\boldsymbol{H}_i), \end{cases} \tag{2}$$

where $\hbar$ is the Planck's constant and $\boldsymbol{H}_i = [\sum_j(J_{ij}(\boldsymbol{R})\boldsymbol{S}_j + \boldsymbol{D}_{ij}(\boldsymbol{R})\times\boldsymbol{S}_j) + g\mu_{\rm B}\boldsymbol{H}_{\rm ext}]$ is the effective field governing the motion of the ith spin. As seen from Eq. (2), the spin-lattice coupling is carried out through $J_{ij}(\boldsymbol{R})$ and $\boldsymbol{D}_{ij}(\boldsymbol{R})$. The action of $\mathcal{H}_{\rm env}$ is usually taken as the form of Langevin-type heat bath, with fluctuation and dissipation terms involved. Here, γ_i^L and γ_i^S are the friction coefficients for lattice and spin motions, respectively, representing the dissipation; the random force $\boldsymbol{f}_i(t)$ and random field $\boldsymbol{h}_i(t)$ are the Gaussian-type stochastic interactions for the lattice and spin motions, respectively, representing the fluctuations, i.e.,

$$\begin{cases} \langle f_{i\alpha}(t)\rangle = 0 \ \text{ and } \ \langle f_{i\alpha}(t)f_{j\beta}(t')\rangle = 2m_i\gamma_i^L k_{\rm B}T\delta_{ij}\delta_{\alpha\beta}\delta(t-t') \\ \langle h_{i\alpha}(t)\rangle = 0 \ \text{ and } \ \langle h_{i\alpha}(t)h_{j\beta}(t')\rangle = 2\hbar\gamma_i^S k_{\rm B}T\delta_{ij}\delta_{\alpha\beta}\delta(t-t'), \end{cases} \tag{3}$$

following the classical fluctuation-dissipation theorem at steady state [41]. By solving the coupled equation of motion in Eq. (2), the canonical phase trajectory of the spin-lattice coupled system described by Eq. (1) could be obtained, from which the thermodynamic observation can be calculated following the statistical thermodynamics.

B. Empirical potential for interatomic interactions of lattice and spin

In our calculations, the nonmagnetic interatomic interaction has taken the form of a Lenard-Jones pairwise potential as

$$U(\boldsymbol{R}) = U(|\boldsymbol{R}_{ij}|) = E_c\left[\left(\frac{R_{ij}}{a}\right)^{-12} - 2\left(\frac{R_{ij}}{a}\right)^{-6}\right], \tag{4}$$

where $R_{ij} = |\boldsymbol{R}_{ij}| = |\boldsymbol{R}_i - \boldsymbol{R}_j|$ is the atomic distance between the ith and jth atoms; $E_c = 4.0$eV denotes the cohesive energy of each particle and $a = 4.56$ Å is the lattice constant at 0 K [42], both of which are set to ensure the calculated bulk modules to be consistent with experimental measurement [43], i.e., $B = 167$ GPa. On the other hand, the net magnetic moment for each particle is written as $|\boldsymbol{M}| = g\mu_{\rm B}|\boldsymbol{S}|$, with the spin magnitude fixed as $|\boldsymbol{S}| = 1$. The

TABLE I. The fundamental parameters of MnSi used in the developed empirical interatomic potential.

	B [GPa]	a [Å]	E_c [eV]	T_C [K]	J_0 [meV]	R_c [Å]	b
This paper	167	4.560	4.0	28.5	0.817	8.509	0.4
Reference	167 [43]	4.559 [42]	-	28.5 [44]	-	-	0.4 [45]

lattice-configuration-dependent exchange interaction function $J_{ij}(\boldsymbol{R})$ is assumed to be the isotropic pairwise form following Ref. [36], as

$$J_{ij}(\boldsymbol{R}) = J_{ij}(|\boldsymbol{R}_{ij}|) = J_0 \cdot \left(1 - \frac{R_{ij}}{R_c}\right)^3 \Theta(R_c - R_{ij}), \quad (5)$$

where $R_c = 8.509$ Å, the cut-off distance including the second-nearest-neighbor spin-spin interactions; $J_0 = 8.19$ MeV is a fitting parameter to ensure the calculated Curie temperature of ferro/paramagnetic phase transition to be the one of experimental measurement for MnSi, i.e., $T_c \approx 28.5$ K [44], and $\Theta(x)$ is the Heaviside step function. For convenience, the DMI strength $\boldsymbol{D}_{ij}(\boldsymbol{R})$ takes a similar form as $J_{ij}(\boldsymbol{R})$:

$$\boldsymbol{D}_{ij}(\boldsymbol{R}) = [bJ_{ij}(\boldsymbol{R})]\hat{\boldsymbol{R}}_{ij}. \quad (6)$$

Here, the lattice configuration dependence of $\boldsymbol{D}_{ij}(\boldsymbol{R})$ is set as same as that of $J_{ij}(\boldsymbol{R})$, and its direction is set parallel to the unit vector of atomic displacement $\hat{\boldsymbol{R}}_{ij}$, where $b \approx 0.4$ [45] is a so-called D/J-ratio determining the size of the skyrmions. Table I lists the parameters used to generate the interatomic potentials for spin and lattice degrees of freedom for MnSi. In principle, the lattice interatomic potential $U(\boldsymbol{R})$ or the spin-spin interaction strengths $J_{ij}(\boldsymbol{R})$ and $D_{ij}(\boldsymbol{R})$ should be fitted from *ab initio* calculation based on density-functional theory. However, such a simplified treatment in the current paper could ensure achieving the fundamental mechanical and magnetic features of MnSi, a typical skyrmion material, which could provide the qualitative understanding of magnetomechanics originated from spin-lattice coupling.

To sum up, on the basis of the proposed SLD scheme [36], we introduced a DMI term written in terms of vector cross of the atomic spins to represent the intrinsic spin-orbit coupling for the electrons expressing magnetism involved in the magnetic atoms, which is the step to coarse grain the information of the electronic level to the atomic level. On the atomic scale, the spin-lattice coupling is expressed in terms of the interdependence of the interaction terms of atomic spins and lattices, giving rise to the intrinsic magnetic-mechanical coupling through the statistical thermodynamics principle used in the SLD simulation scheme, which is the step to coarse grain the information of the atomic level to the macroscopic level.

III. ATOMISTIC SIMULATION DETAIL

For the calculation of magneto-mechanical properties, the simulation box is set to contain 20 simple-cubic unit cells along each dimension of Cartesian coordinate system, with periodic boundary condition applied to avoid the surface effects. The phase-space trajectories, i.e., $s(t) = \{\boldsymbol{R}_i(t), \boldsymbol{p}_i(t), \boldsymbol{S}_i(t)\}$, are obtained by solving the equation of motion presented in Eq. (2) using velocity-Verlet approach [46] with a time step as 0.4 fs. To achieve a stable magnetic phase, the spin subsystem of the spin-lattice coupling system is initialized at extremely high temperature, e.g., $\sim 10^4$ K, and then relaxed for 400 ps upon an isothermal-isobaric (NPT) ensemble [47] to obtain an equilibrium volume of the interested systems under a specific applied external magnetic field $\boldsymbol{H}_{\text{ext}}$ along the out-of plane direction, ranging from 0 to $3H_0$ (Here $H_0 = 0.0397$ T, see Table II). The temperature and external stress of the NPT ensemble are kept as 25 K and 0 GPa, respectively, using the Langevin thermostat and Bredensen barostat [36]. Then, another 400-ps SLD run is performed to collect the phase-space trajectory for the calculation of thermodynamic observations. All the simulations are repeated at least ten times to limit the statistical error. It is checked that doubling the size of the simulation box or relaxation time gives rise to the error smaller than 2%. As a schematic in Fig. 2, there are several magnetic-order phases existing with increasing H_{ext} (here, $H_{\text{ext}} \equiv |\boldsymbol{H}_{\text{ext}}|$), i.e., H phase with $H_{\text{ext}} < 0.75H_0$, Skx phase with $0.75H_0 < H_{\text{ext}} < 1.10H_0$, C phase at $1.10H_0 < H_{\text{ext}} < 1.80H_0$, and F phase at $H_{\text{ext}} > 1.80H_0$. Note that the propagation direction of the spiral spin textures $\boldsymbol{Q}$ in H and C phases is parallel to $\boldsymbol{H}_{\text{ext}}$, while the triple $\boldsymbol{Q}$ direction of skyrmions is perpendicular to $\boldsymbol{H}_{\text{ext}}$. and the magnetostriction direction is always along the $\boldsymbol{Q}$ direction with out of plane for H and C phases and in plane for Skx phase, there is no magnetostriction for the F phase due to the isotropic parallel spin configuration.

IV. RESULTS AND DISCUSSION

Because of the intrinsic spin-lattice coupling in skyrmion materials, the mechanical properties are found to be sensitive with the change of magnetic ordering. In our simulation on the basis of the modified SLD model, increasing the external field $\boldsymbol{H}_{\text{ext}}$ results in the magnetic-ordering phase transitions from H to F phases. In this following, we will present the quasi-static and dynamical responses of mechanical properties in MnSi, such as magnetoexpansivity and magnetoelasticity, magnetic-induced local distortion of lattice structure and the relaxation time of lattice system. Here, all the values of physical quantities presented in this section are normalized to the corresponding characteristic ones for MnSi, as listed in Table II.

TABLE II. Characteristic values of thermodynamic properties of MnSi.

	H_0 [T]	C_0 [GPa]	ω_D [MeV]	τ_D [ps]
This paper	0.0397	283.3	56.87	0.115
Reference	-	283.0 [54]	56.87 [42]	0.115 [42]

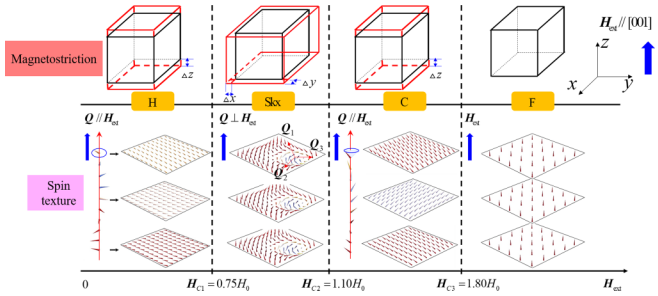

FIG. 2. Schematics of magnetic ordering changes with increasing applied magnetic field H_{ext}, from H with $H_{\text{ext}} < H_{C1}$, Skx with $H_{C1} < H_{\text{ext}} < H_{C2}$, C with $H_{C2} < H_{\text{ext}} < H_{C3}$, to F phases with $H_{\text{ext}} > H_{C3}$. Here, $H_{C1} = 0.75H_0$, $H_{C2} = 1.10H_0$ and $H_{C3} = 1.80H_0$ with $H_0 = 0.0397$T. The H phase and C phase have a propagation direction along z direction which is the magnetostriction direction along, i.e., out-of-plane direction, and the triple-Q propagation direction of Skx phase is perpendicular to z direction, i.e., in-plane direction with in-plane magnetostriction. The F phase has no magnetostriction for the isotropic parallel spin configuration.

A. Global magnetomechanics

The mechanical properties change with the magnetic ordering induced by H_{ext}, namely magnetomechanics, could be represented by magnetovolume Ω, magnetostriction λ and magnetoelasticity ϕ_{ij}, respectively, defined as [48]

$$\Omega = \frac{\Delta V}{V_0} = \frac{V(H_{\text{ext}})}{V_0} - 1,$$
$$\lambda = \frac{\Delta a}{a_0} = \frac{a(H_{\text{ext}})}{a_0} - 1, \tag{7}$$
$$\phi_{ij} = \frac{\Delta C_{ij}}{C_0} = \frac{C_{ij}(H_{\text{ext}})}{C_0} - 1,$$

where $V(H_{\text{ext}})$, $a(H_{\text{ext}})$, and $C_{ij}(H_{\text{ext}})$ are the volume, lattice constant, and elastic constants under the applied field H_{ext}, respectively, with V_0, a_0, and C_0 as the corresponding ones in the F phase. On the other hand, their coefficients α, β, and χ_{ij} are usually defined to denote the rate of mechanical property changes with H_{ext}, respectively, as [48]

$$\alpha = \left(\frac{\partial \Omega}{\partial H_{\text{ext}}}\right)_{T,P}, \quad \beta = \left(\frac{\partial \lambda}{\partial H_{\text{ext}}}\right)_{T,P}, \quad \chi_{ij} = \left(\frac{\partial \phi_{ij}}{\partial H_{\text{ext}}}\right)_{T,P}. \tag{8}$$

Here, the subscripts T and P represent the isothermal and isobaric conditions for the NPT ensemble. Moreover, the elastic constants C_{ij} are estimated in the following:

$$C_{ij} = \frac{1}{V}\frac{\partial^2}{\partial \varepsilon_{ij}^2}[U(\varepsilon_{ij}; H_{\text{ext}})], \tag{9}$$

where ε_{ij} is the applied external strain and $U(\varepsilon_{ij}; H_{\text{ext}})$ is the potential energy of the system by applying ε_{ij} under H_{ext}. Here, only the elastic constants along the principal directions, i.e., C_{11} and C_{33}, respectively, along [100] and [001] directions, are calculated to compare with the experimental measurement in Ref. [49].

Figure 3(a) presents Ω, as well as its coefficient α, as functions of H_{ext}, respectively. As known, the ferromagnetic

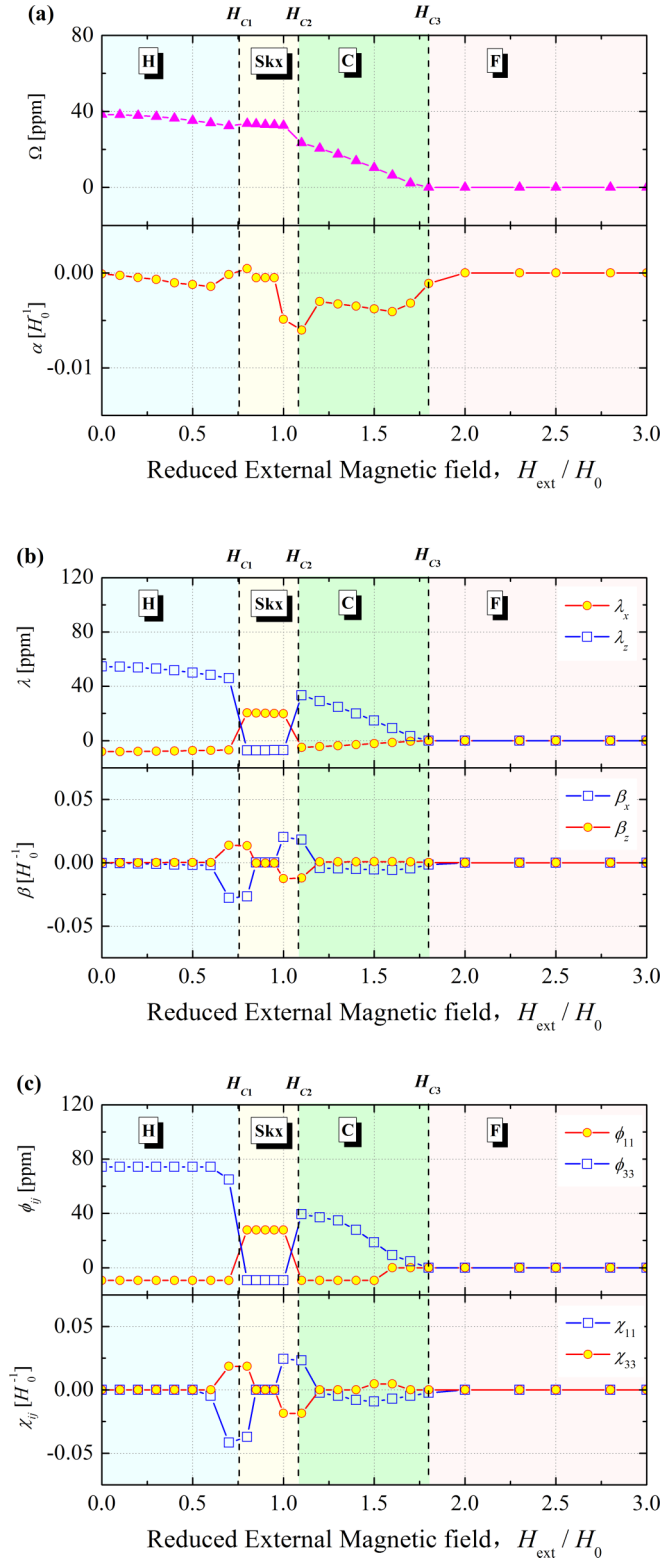

FIG. 3. Properties of magnetomechanics of skyrmion materials varying with external field H_{ext}, e.g., (a) magnetovolume Ω, (b) magnetostriction λ, (c) magnetoelasticity ϕ_{ij}, and their coefficients.

spin-spin interaction results in an isotropic contraction for the lattice structure via the spin-lattice coupling [36]. Due to the presence of DMI in skyrmion materials, e.g., MnSi, the competition between the DMI and HEI gives rise to the

nonalignment for the neighboring spins. In general, the applied external field reduces the spin nonalignment and forces the spins to be parallel with $\boldsymbol{H}_{\text{ext}}$. Therefore, the stronger is the applied field, the weaker is the spin nonalignment, leading to the phase transition of magnetic ordering from H to F, thus enhancing the contraction of volume, as plotted in Fig. 3(a). However, the value of defined magnetovolume Ω is the synergistic result of the competition between intrinsic spin-spin interaction and the mechanical properties of skyrmion materials, e.g., Ω has a stable value of ∼40 part-per-million (ppm) at H and Skx phases with $H_{\text{ext}} < 1.10H_0$, but gradually decays to be zero in the C phase with H_{ext} growing up to $1.80H_0$. Seen from the magnetovolume coefficient α plotted in Fig. 3(a), it shows a negative value at all phases of magnetic ordering considered here, arising from the fact of lattice contraction due to the enhanced spin alignment with increasing applied field, and the fluctuation is significant in the phases of Skx and C, in particular near the corresponding phase boundary, where there is an absolute maximum $|\alpha| \sim 60 \times 10^{-6} H_0^{-1}$.

It should be noted that the anisotropic nature of DMI in skyrmion materials can result in the anisotropic spin nonalignment in skyrmion materials, thus inducing the anisotropic mechanical properties via spin-lattice coupling. Besides the contraction similar to that revealed in Ω due to the spiral magnetic ordering, both λ and ϕ_{ij} plotted in Figs. 3(b) and 3(c) show the same anisotropic feature in the magnetic phases having nonalignment spin texture due to the competition of DMI against HEI and ZI. As in the weakening of such spin nonalignment by increasing H_{ext}, the anisotropy of both λ and ϕ_{ij} reduce to be zero in F phase. In the H and C phases, the significant spin nonalignment is found along the same propagation direction of the spiral spin texture, i.e., out-of-plane in our simulations. Therefore, the lattice structure elongates along the out-of-plane and shrinks along in-plane direction, i.e., $\lambda_z > 0 > \lambda_x$, so does the elasticity, i.e., $\phi_{33} > 0 > \phi_{11}$. However, the most spin nonalignment is present along the direction parallel to the so-called triple $\boldsymbol{Q}$ direction in the Skx phase, i.e., the in-plane direction in our simulations, so the reversal of anisotropic features of both λ and ϕ_{ij} are indicated in Fig. 3(b) and 3(c), i.e., $\lambda_x > 0 > \lambda_z$ and $\phi_{11} > 0 > \phi_{33}$, respectively. This anomalous magnetomechanical phenomenon in the current paper is qualitatively consistent with the experimental measurement for the elastic constant of MnSi [49]. As seen from Fig. 3(b), $|\lambda|_{\text{max}} \sim 55$ ppm, which is comparable with that in most traditional ferromagentic materials, such as ferrites (Fe_3O_4, $|\lambda|_{\text{max}} \sim 40$ ppm) [48]. The coefficients of magnetostriction β and elasticity χ_{ij} have significant fluctuations near both sides of the Skx phase boundaries, because of the anisotropy reversion. In addition, the magnetic ordering and phase transition could be modulated by the strength of DMI, so is the spin nonalignment. Here, D/J ratio b varies artificially to check its effects on magnetomechanical properties. Plotted in Fig. 4(a), increasing b requires a larger external field to maintain the chiral magnetic ordering, giving rise to the corresponding variation of anisotropic magnetostriction, denoting by λ_x and λ_z, respectively, plotted in Figs. 4(b) and 4(c). From the results shown in Figs. 3 and 4, the potential skyrmion-based magnetomechanical device is possible based on the magnetic order transition from H to Skx phases, or from Skx to C phases. Further, the intrinsic anisotropic DMI

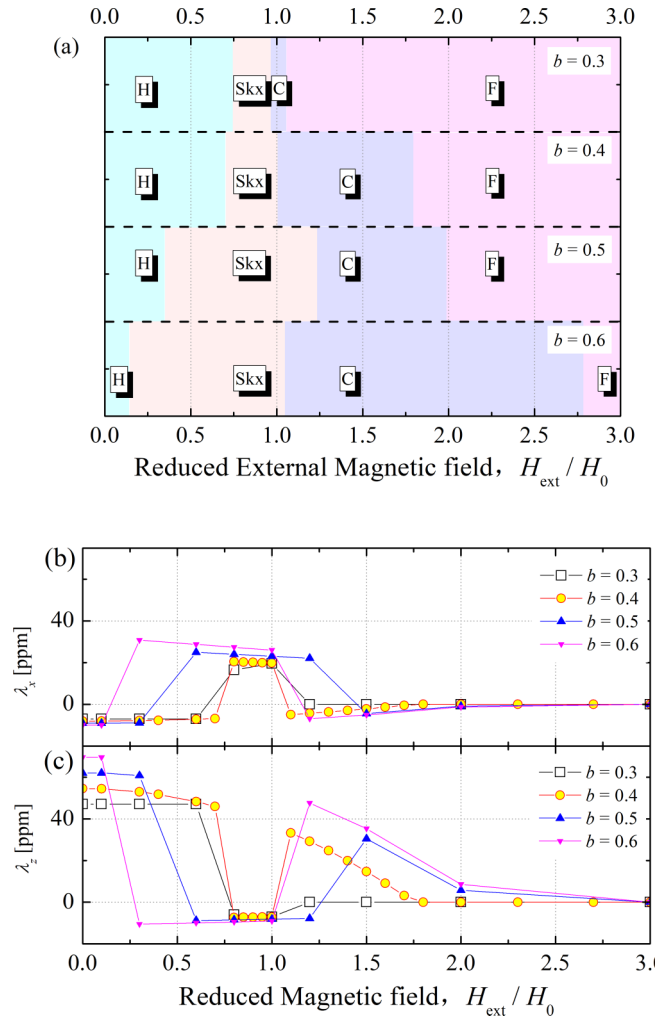

FIG. 4. (a) The magnetic phases with increasing applied magnetic field at various b, (b) magnetostriction λ_x, and (c) λ_z changes with magnetic field for various b.

is responsible for the spiral spin texture, thus the anisotropic mechanical properties in skyrmion materials via spin-lattice coupling effects.

Note that researchers claimed that the magnetic-induced anisotropy in mechanical properties is owed to spin-orbit coupling [49] only (represented by DMI in our model), but no significant contribution is found from HEI, which presents a different physical picture revealed in the current atomistic study. Based on our proposed atomic Hamiltonian in Eq. (1), an analytical expression is derived to describe the anisotropic feature of elasticity [50]. In particular, as presented in Sec. II of the Supplemental Material [50], the internal stress of the spin-lattice-coupled system shows that the mechanical properties are determined by the competition between lattice-lattice elastic interaction and the extra spin-lattice interaction induced by the specific magnetic ordering. The anisotropic mechanical properties are the result of the synergistic effects of the intrinsic spin and lattice interactions in skyrmion materials, where DMI stabilizes the spiral spin texture; then the competition between DMI and HEI (as well as ZI) determines the nonalignment and chirality of the whole

spin system, and finally the competition between spin-lattice interaction and elastic interaction of lattice leads to anisotropy of mechanical properties. Here, the functional forms of lattice-configuration-dependent DMI and HEI are the key determinants of the anisotropic nature. In this regard, compared to the LLG model, the proposed atomistic model could give a clear microscopic physical picture of the magnetomechanical phenomena in skyrmion materials, which could also provide the microscopic understanding of the phenomenological parameters that characterize the magnetic-mechanical coupling used in the LLG model. Similar synergistic effects could also be found in the magnetic-induced local distortion of lattice structure discussed in the following.

B. Local distortion of lattice structure induced by spiral magnetic ordering

For an arbitrary atom located in the symmetrical center of the lattice structure, it would exert an imbalanced interatomic force provided by its neighboring spins because of the noncentral symmetrical nature of DMI, which, meanwhile, is enhanced by the presence of spiral-spin arrangement in the nonferromagnetic phase, especially for Skx phases which have a strong nonaligned spin configuration at the center and boundary region of skyrmions. Therefore, besides the global mechanical deformation, the chiral spin texture due to the presence of DMI in skyrmion materials could also give rise to the local distortion of lattice structure (short for lattice distortion). Accordingly, the so-called slip-vector $\boldsymbol{d}$ is usually defined to characterize the nonsymmetrical feature of a local environment of lattice arrangement for a specific atom in atomic simulations [51] as

$$\boldsymbol{d}_i = \frac{1}{n_i} \sum_{j \in NN} \left(\frac{\boldsymbol{R}_{ij}}{a_0} \right), \tag{10}$$

where $\boldsymbol{d}_i$ is the slip-vector of the ith atom, a_0 is the lattice constant in the F phase, $\boldsymbol{R}_{ij}$ is the atomic displacement between the ith and jth atoms, and n_i is the number of neighboring atoms of the ith atom. Here, the summation of $j \in NN$ in Eq. (10) includes the neighboring atoms up to the second-nearest neighbors (2nd-NN) [51]. In particular, if an atom locates at the geometrical center of the box made up by its neighboring atoms, we have $\boldsymbol{d}_i = 0$, because there are always pairwise atoms in its neighborhood, e.g., j and j', with $\boldsymbol{R}_{ij'} = -\boldsymbol{R}_{ij}$.

In the following, the slip-vector fields $\{\boldsymbol{d}_i\}$ in four Skx phases under different applied external fields are demonstrated to clarify the atomistic physical picture of lattice distortion. First, following the magnetic phase diagram in Fig. 2, four spin configurations are obtained under $H_1 = 0.80H_0$, $H_2 = 0.85H_0$, $H_3 = 0.90H_0$, and $H_4 = 1.00H_0$, respectively, in a simulation box containing $120 \times 25 \times 10$ simple cubic unit cells. Fixing the spin configuration, the lattice atoms are then quenched until all the atomic forces are zero so as to obtain a stable lattice configuration, based on which the slip vectors for each atom are calculated following Eq. (10). Plotted in Figs. 5(a), 5(c), 5(e), and 5(g), respectively, the in-plane schematics of spin configuration under various H_{ext} mentioned above, where the color textures denote the out-of-plane components of atomic spins, i.e., S_z, and the black arrows represents the in-plane spin components. The corresponding slip vectors of each atom, i.e., $\{\boldsymbol{d}_i\}$ normalized by $d_{\max} = 349.0$ ppm, under the specific spin configuration are respectively shown in Figs. 5(b), 5(d), 5(f), and 5(h), where the color textures denote the strength of $\{\boldsymbol{d}_i\}$, and the red arrows represent the length of its in-plane component. Seen from spin configurations under a specific H_{ext}, the spatial variation of the spin nonalignment is the strongest near boundary of the adjunct skyrmions and the center of each skyrmion, giving rise to the significantly large values of $\boldsymbol{d}_i$, no matter to in-plane or out-of-plane components. Further, consistent with the calculation results based on LLG equations [35], increasing H_{ext} reduces the number and size of skyrmions, so as to enhance the spatial variation of the spin nonalignment, thus a larger strength of $\{\boldsymbol{d}_i\}$. On the other hand, the in-plane component of $\{\boldsymbol{d}_i\}$ directs to the skyrmions center, indicating an attractive interatomic force provided by skyrmions to its center, and the density of arrows found near the boundary region among skyrmions suggests that there is a repulsive interatomic interaction. In addition, the lattice local distortion distribution induced by the H and C phases in a simulation box containing $20 \times 20 \times 100$ simple cubic unit cells, respectively, under $H_{\text{ext}} = 0.3H_0$ and $H_{\text{ext}} = 1.3H_0$, are present in Figs. 6(a) and 6(b), with the corresponding magnetic ordering along xz and yz planes, aiming to show

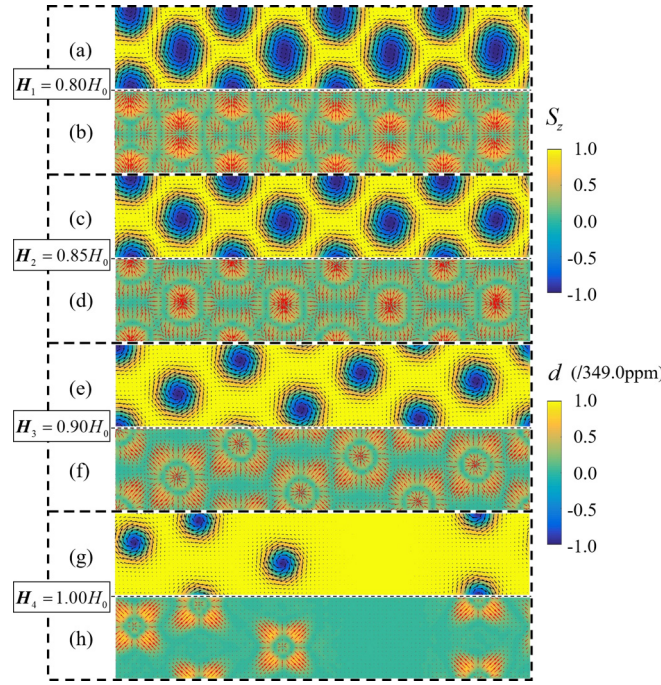

FIG. 5. The diagram of skyrmion lattice spin texture and the corresponding local lattice distortion distribution characterized by slip vector. Figures 3(a), 3(c), 3(e), and 3(g) are the skyrmion spin texture under different external magnetic fields with $H_1 = 0.80H_0$, $H_2 = 0.85H_0$, $H_3 = 0.90H_0$, and $H_4 = 1.0H_0$, the black arrows represent the components of spin in xy plane, while the contour denotes the values of spin component S_z. Figures 3(b), 3(d), 3(f), and 3(h) are the corresponding slip vectors under different magnetic configurations, the contour represents the strength of the slip vector, which is normalized by 349.0 ppm, and the red arrows indicate the in-plane slip vector components.

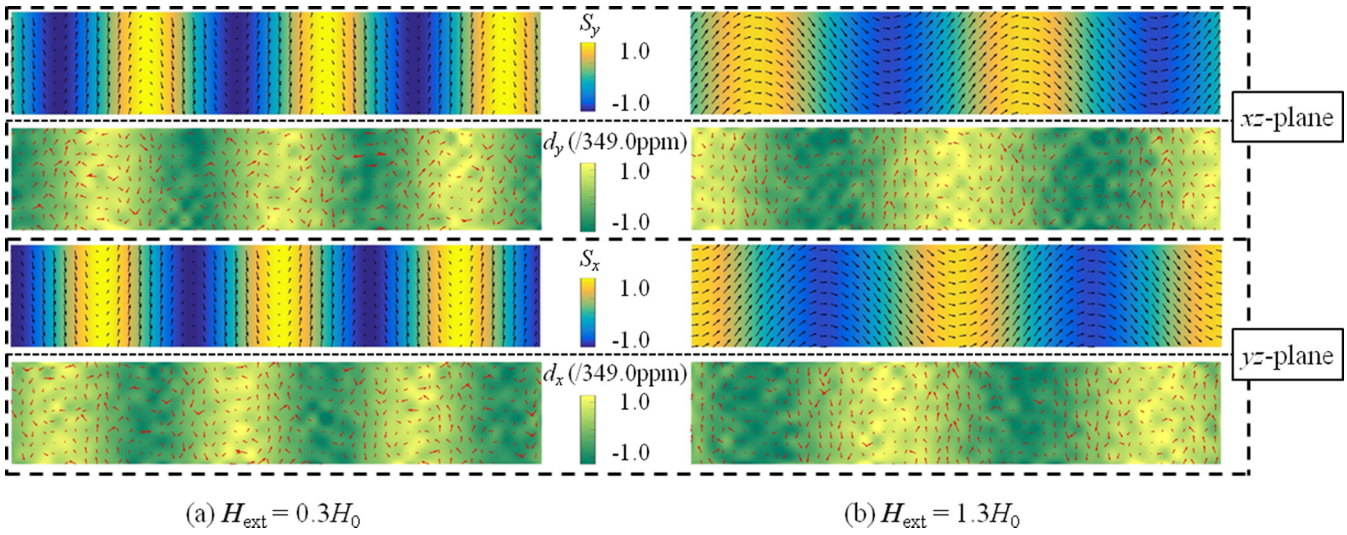

FIG. 6. The diagram of chiral magnetic ordering in (a) H phase ($H_{ext} = 0.3H_0$) and (b) C phase ($H_{ext} = 1.3H_0$), respectively, on the xz and yz planes, with the corresponding slip-vector field denoting the local lattice distortion induced by spin nonalignments. The symbols shown here are similar to those in Fig. 5.

that the lattice distortion is closely related to the magnetic structure characteristics for the propagation direction of spiral lattice distortion being parallel to the propagation direction of magnetic ordering, i.e., out of plane. Note that the different geometrical distribution of lattice distortion might determine the kinetic aspect of magnetic-induced mechanical properties in skyrmion materials, which will be discussed in the following section.

In this regard, as the result of magnetomechanics effects via the intrinsic spin-lattice coupling, the lattice distortion is arising from the spin nonalignment induced by DMI, so a strain field has to be introduced to describe such lattice distortion in the phenomenological models based on the LLG equation [35]. However, based on the analysis shown in the Supplemental Material [50], $\{\boldsymbol{d}_i\}$, induced by DMI has a maximum value of 18.87 ppm, only ∼6% of current simulation results (349.0 ppm) shown in Fig. 5, which again indicates that the anomalous magnetomechanical properties in skyrmion materials are not only from spin-orbit coupling, i.e., DMI in the current paper, but the synergistic effects of HEI, ZI, and elastic interactions. In addition, the morphology of local distortion of lattice structure relies on the form of DMI and the dependence of $D_{ij}(\{\boldsymbol{R}_i\})$ on the lattice configurations. Our current simplified model could only give a qualitative result, which, however, might provide a microscopic understanding of the physical picture of lattice responses due to the change of magnetic ordering.

C. The dynamic responses of lattice to the magnetic ordering change

The global anisotropy and local distortion of lattice structure are two important thermodynamic aspects of magnetomechanics in skyrmion materials, showing the application possibility on magnetic-tunable mechanical devices [23]. Note that mechanistic understanding of the dynamic response of the lattice configuration due to the magnetic ordering change is quite an important issue in the aspect of materials engineering as well as fundamental physics. In the following, we will discuss the dynamic response of lattice if the magnetic ordering is changed by applied external field.

From the point of view in thermodynamics, the magnetic-induced global anisotropy and local distortion are the result of free-energy minimization of the coupled spin-lattice system in skyrmion materials, where the work done on external magnetic field acted on the spin subsystem is transferred into the internal energy stored in spin and lattice subsystems, accompanied by the heat dissipation. According to statistical thermodynamic theory, the heat is stored in the form of the thermal vibrations of atomic lattices and spins at finite temperatures, respectively, named phonon and magnon, both of which are keeping thermodynamics equilibrium under certain external conditions via spin-lattice coupling. If there is work done externally on the spin-subsystem, for instance, increasing the applied external magnetic field, the spin-subsystem will reach another new equilibrium state by modulating the magnon modes and their thermal distribution. Meanwhile, the energy would also transfer from spin- to lattice-subsystem through spin-lattice coupling, bringing the lattice-subsystem to the new equilibrium state by modulating the distribution of phonon modes. In this regard, the magnetomechanical responses are in fact the kinetic process in the atomistic scale. Following Boltzmann's transformation theory [52], the so-called relaxation time τ is defined to characterize the speed of this kinetic process. Recently, Wen *et al.* [53] proposed an equation to measure τ of an isolated many-body system with an ensemble of interactive phonons, which is associated with the decay time of the reduced kinetic energy $T(t)$ when such system relaxes towards its new equilibrium state, i.e.,

$$T(t) = T_f[1 + \exp(-2t/\tau)\cos(2\omega t + \varphi)], \qquad (11)$$

where T_f is the kinetic energy of the new equilibrium state, τ is the characteristic relaxation time, denoting the speed of heat dissipation, ω is the effective vibrational frequency of the

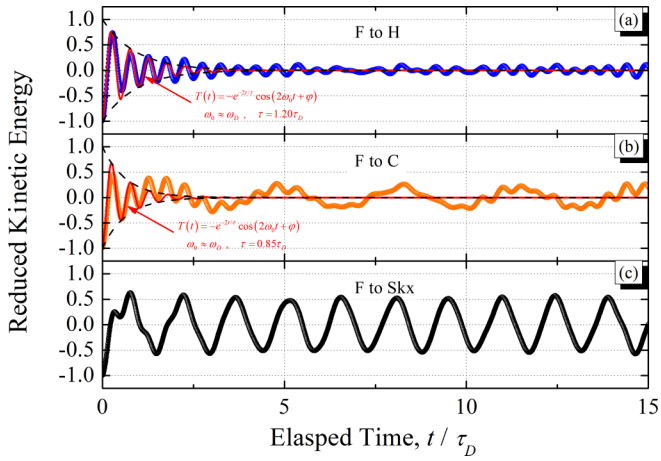

FIG. 7. The reduced kinetic energy $T(t)/T_f$ of an adiabatic relaxation process for lattice response to the chiral spiral spin texture. (a) The blue points are the simulation results for the lattice relaxation process from the equilibrium configuration at F phase to that at H, fitting by $T(t) = -e^{2t/\tau}\cos(2\omega_0 t)$ (red line), with $\omega_1 = \omega_D$ and $\tau_1 = 1.20\tau_D$, and black dashed line is the envelop of $\pm(e^{-2t/\tau_1})$. (b) The similar simulation results from F to C phase is plotted by orange points, fitting with $\omega_2 = \omega_D$ and $\tau_2 = 0.85\tau_D$, and pink dashed line is the envelop of $\pm(e^{-2t/\tau_2})$. (c) The black points are the simulation results from F to Skx phase.

phonon modes involved during the kinetic process, and φ is the phase-angle.

To clarify the physical picture of the dynamic responses of lattice, we calculate the corresponding characteristic relaxation time τ due to the magnetic ordering change, e.g., from F phase to H, C and Skx phases, respectively. Note that only the responses related to local distortion of lattice-subsystem is considered in our simulation, because the global mechanical responses could be expressed in terms of the localized lattice coordinates. Here, an undistorted lattice configuration equilibrated corresponding to the magnetic ordering at F phase is generated beforehand. Then, by fixing the spin configuration at a specific spiral magnetic ordering, the lattice-subsystem is adiabatically relaxed, i.e., without attaching to the external environment, where the time dependence of the reduced kinetic energy $T(t)/T_f$ is collected. Following Eq. (11), the characteristic relaxation time τ could be obtained.

Figures 7(a), 7(b) and 7(c) plot $T(t)/T_f$ of the lattice subsystem for the kinetic processes to H, C, and Skx phases, respectively, starting from F phase. Here, $T(t)$ in the first two processes, i.e., F to H and F to C, shows the typical underdamped oscillation behavior, indicating the lattice subsystem can reach the new equilibrium state in current simulation time, $t < 5\tau_D$, with $\tau_D = 11.5$ fs as the reciprocal of Debye frequency of MnSi. According to Eq. (11), the relaxation time τ for the processes of F to H and F to C as $\tau = 1.20\tau_D$ and $\tau = 0.85\tau_D$, respectively. Meanwhile, the fitting effective oscillation frequency $\omega \approx \omega_D$ from F to H and F to C suggests that the processes are mainly owed to the kinetics of phonon modes. However, for the process from F to Skx, $T(t)$ shown in Fig. 7(c) does not illustrate a significant damping evolution behavior, so τ could not be obtained in this case. In other words, the response speed of lattice from F to H and C is faster than F to Skx. In those relaxation processes, it is actually a redistribution process of the phonon mode, and the mean lifetime of the phonons participating in the relaxation process will determine the characteristic relaxation time of the corresponding relaxation process, which, as defined here, is the lattice response speed related to in the magnetic ordering phase transition.

In the microdynamic point of view, the heat dissipation is by means of the energy and momentum transfer between phonons, so that the speed of heat dissipation is determined by the lifetime of participated phonon modes during the corresponding kinetic process. Following Ref. [53], the kinds and proportion of phonon modes participating in the heat dissipation during the kinetic process could be checked from the Fourier transformation $\kappa(\omega)$ of $T(t)$, i.e., $\kappa(\omega) = \int T(t)e^{-i\omega t}dt$. Figures 8(c), 8(d) and 8(e), respectively, plot $\kappa(\omega)$ for the corresponding processes mentioned in Fig. 7, as well as the comparison with dispersion relation $\omega = \omega_{k\sigma}$ and density of states $g(\omega)$ of phonon modes at the F phase for MnSi. Here, the subscripts k and σ represent the wave vector and the occupation number of phonon respectively, all the terms with respect to ω are normalized by the Debye frequency $\omega_D = 56.87$ MeV of MnSi. As plotted in Fig. 2, the spin nonalignment along the out-of-plane direction is enhanced from F to H and F to C magnetic phase transitions, giving rise to the out-of-plane propagated local distortion of lattice structure as showed in Fig. 6, thus requires the participation of phonon modes with wave vector of [001] [the phonon modes from Γ point to X point of the Brillouin zone shown in Fig. 8(a)], corresponding to the peaks of $\kappa_1(\omega)$ and $\kappa_2(\omega)$ near ω_D in Figs. 8(c) and 8(d). Comparing to $\kappa_1(\omega)$, $\kappa_2(\omega)$ have an extra large peak in the low-frequency region, indicating that it requires the phonon modes with long wavelength participating in the kinetic process to establish the lattice distortion corresponding to the spin configuration at the C phase, which requires further investigation to check if there is long-range correlation between the local lattice structure. Note that, compared to $\kappa_3(\omega)$ whose the low-frequency peak is predominant feature of kinetic process, more phonon modes near the boundary of the Brillouin zone are participating in the relaxation process for $\kappa_1(\omega)$ and $\kappa_2(\omega)$, respectively, from F to H and C. Note that these phonons near the Brillouin boundary are more susceptible to be scattered, so they can reach a new stable distribution much faster, giving rise to the smaller characteristic relaxation time. In addition, from the configuration of the lattice under different magnetic ordering, the local noncollinear skyrmion magnetic structure with 3Q in-plane propagation induces a similar in-plane local lattice distortion, as shown in Fig. 5. The H and C phases propagating along the out-of-plane direction with a single Q also induce a spiral localized lattice distortion that also propagates out of plane. Thus, the difference of the distributions of local lattice distortion may give rise to a different response speed of lattice, and it may take more time for lattice to reach a more complex configuration with local lattice distortion of Skx phase than the relatively simpler configurations of H and C phases. Therefore, the response speed of lattice to magnetic ordering change for F to H and F to C is faster than that for F to Skx.

In this regard, the kinetic process illustrated in Figs. 7 and 8 suggests that the characteristic time for lattice response to the

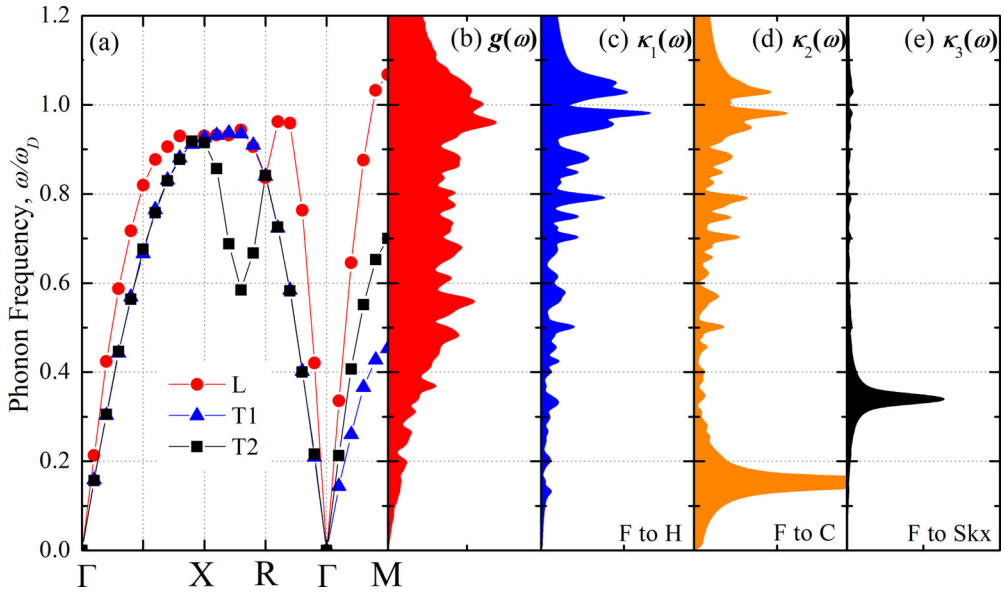

FIG. 8. The phonon dispersion relation $\omega_{k\sigma} = \omega_k$ and (b) density of states of spin-lattice dynamic systems, here L (red solid circles), T1 (blue triangle), and T2 (black squares) represent the three branches of phonon mode for a given wave vector. (c) The phonon mode spectrums κ_1, κ_2, and κ_3 participating in the relaxation process are shown in Figs. 7(c), 7(d), and 7(e), obtained by applying Fourier transform on $T(t)$ in Figs. 6(a), 6(b), and 6(c), respectively.

magnetic ordering change is of the order of Debye relaxation time, which is determined by the mean lifetime of phonon modes participating. In addition, the response speed of lattice to magnetic ordering change for F to Skx is much slower than those for F to H and F to C, indicating a weaker effect between lattice and magnetic ordering in the Skx phase, thus a lower heat dissipation or a lower energy consumption, which might be the reason why a rather smaller electric current is required to drive the diffusion of skyrmions than the case of driving the traditional magnetic domains.

V. CONCLUSION

In this paper, taking the typical B20-type MnSi for an example, we applied the developed SLD model on skyrmion materials with the anisotropic DMI involved, by constructing a pairwise Lennard-Jones potential for lattice dynamics, and pairwise form of the lattice-configuration-dependent Heisenberg exchange integral function and DM function to describe the spin-lattice coupling effects. Based on this modified SLD model, we calculate the magnetic-induced mechanical anisotropy, i.e., magnetovolumetric, magnetostriction, and magnetoelastic properties, which is found to be qualitatively consistent with the experimental measurement [49]. In this regard, this atomic simulation model is, in principle, appropriate for the theoretical analysis of the thermodynamics, magnetics, and mechanics of skyrmion materials. Besides, we also clarify the physical picture of the thermodynamics (i.e., global mechanical anisotropy and local distortion of lattice structure) and kinetics (the characteristic speed of mechanical responses against magnetic ordering change) of magnetomechanics of skyrmion materials in atomistic scale. From the thermodynamics aspect, it is found that the global anisotropy and local distortion are the result of the synergistic effects of all the intrinsic interatomic interactions, i.e., DMI stabilizes the spiral spin texture, then the competition between DMI and HEI (as well as ZI) determines the nonalignment and chirality of the whole spin system, and finally the competition between spin-lattice interaction and elastic interaction of the lattice leads to anisotropy and local distortion of lattice structure. From the kinetics aspect, the relaxation time of lattice structure due to the change of magnetic ordering is proposed to denote the speed of mechanical responses against the magnetic loading, by analyzing the heat dissipation rate corresponding to the redistribution of phonon modes involved. The calculation results indicate that the response speed is quite small in the kinetic process from F to Skx phase, showing a low energetic consumption in driving the diffusion of skyrmions. We hope the current microscopic understanding of magnetomechanics in skyrmion materials could help the research and design of the skyrmion-based spintronic devices.

ACKNOWLEDGMENTS

This work was supported by NSFC (Grants No. 11602310 and No. 11672339) and the Guangzhou Science and Technology Project (Grant No. 201707020002). Y.Z. also acknowledges support from the Special Program for Applied Research on Super Computation of the NSFC-Guangdong Joint Fund (the second phase), Fok Ying Tung Foundation, Guangdong Natural Science Funds for Distinguished Young Scholar, and China Scholarship Council.

[1] I. Dzyaloshinsky, J. Phys. Chem. Solids **4**, 241 (1958).
[2] T. Moriya, Phys. Rev. **120**, 91 (1960).
[3] N. Romming, C. Hanneken, M. Menzel, J. E. Bickel, B. Wolter, K. von Bergmann, A. Kubetzka, and R. Wiesendanger, Science **341**, 636 (2013).
[4] N. Nagaosa and Y. Tokura, Nat. Nanotechnol. **8**, 899 (2013).
[5] Y. Okamura, F. Kagawa, M. Mochizuki, M. Kubota, S. Seki, S. Ishiwata, M. Kawasaki, Y. Onose, and Y. Tokura, Nat. Commun. **4**, 2391 (2013).
[6] W. Chen, L. Liu, Y. Ji, and Y. Zheng, Phys. Rev. B **99**, 064431 (2019).
[7] Y. Nii, T. Nakajima, A. Kikkawa, Y. Yamasaki, K. Ohishi, J. Suzuki, Y. Taguchi, T. Arima, Y. Tokura, and Y. Iwasa, Nat. Commun. **6**, 8539 (2015).
[8] K. Shibata, J. Iwasaki, N. Kanazawa, S. Aizawa, T. Tanigaki, M. Shirai, T. Nakajima, M. Kubota, M. Kawasaki, H. S. Park *et al.*, Nat. Nanotechnol. **10**, 589 (2015).
[9] J. Iwasaki, M. Mochizuki, and N. Nagaosa, Nat. Commun. **4**, 1463 (2013).
[10] H. Y. Yuan and X. R. Wang, Sci. Rep. **6**, 22638 (2016).
[11] X. Z. Yu, N. Kanazawa, W. Z. Zhang, T. Nagai, T. Hara, K. Kimoto, Y. Matsui, Y. Onose, and Y. Tokura, Nat. Commun. **3**, 988 (2012).
[12] G. Finocchio, F. Büttner, R. Tomasello, M. Carpentieri, and M. Kläui, J. Phys. D: Appl. Phys. **49**, 423001 (2016).
[13] C. Pappas, E. Lelievre-Berna, P. Falus, P. M. Bentley, E. Moskvin, S. Grigoriev, P. Fouquet, and B. Farago, Phys. Rev. Lett. **102**, 197202 (2009).
[14] T. Tanigaki, K. Shibata, N. Kanazawa, X. Yu, Y. Onose, H. S. Park, D. Shindo, and Y. Tokura, Nano Lett. **15**, 5438 (2015).
[15] S. X. Huang and C. L. Chien, Phys. Rev. Lett. **108**, 267201 (2012).
[16] X. Yu, Y. Onose, N. Kanazawa, J. Park, J. Han, Y. Matsui, N. Nagaosa, and Y. Tokura, Nature **465**, 901 (2010).
[17] S. Seki, X. Z. Yu, S. Ishiwata, and Y. Tokura, Science **336**, 198 (2012).
[18] S. Heinze, K. Von Bergmann, M. Menzel, J. Brede, A. Kubetzka, R. Wiesendanger, G. Bihlmayer, and S. Blügel, Nat. Phys. **7**, 713 (2011).
[19] F. Jonietz, S. Mühlbauer, C. Pfleiderer, A. Neubauer, W. Münzer, A. Bauer, T. Adams, R. Georgii, P. Böni, R. A. Duine, K. Everschor, M. Garst, and A. Rosch, Science **330**, 1648 (2010).
[20] S. Woo, K. Litzius, B. Krüger, M.-Y. Im, L. Caretta, K. Richter, M. Mann, A. Krone, R. M. Reeve, M. Weigand, P. Agrawal, I. Lemesh, M.-A. Mawass, P. Fischer, M. Kläui, and G. S. D. Beach, Nat. Mater. **15**, 501 (2016).
[21] L. Kong and J. Zang, Phys. Rev. Lett. **111**, 067203 (2013).
[22] K. Everschor, M. Garst, B. Binz, F. Jonietz, S. Mühlbauer, C. Pfleiderer, and A. Rosch, Phys. Rev. B **86**, 054432 (2012).
[23] R. Hilzinger and W. Rodewald, *Magnetic Materials: Fundamentals, Products, Properties, Applications* (Vacuumschmelze, MCD Verlag, Germany, 2013).
[24] Here, the term of *skrymion materials* mentioned in the current paper stands for the materials having skyrmion magnetic structure under certain applied external conditions.
[25] J. Wang, Annu. Rev. Mater. Res. **49**, 361 (2019).
[26] J. P. Joule, London, Edinburgh, Dublin Philos. Mag. J. Sci. **30**, 76 (1847).
[27] C. Kittel, Rev. Mod. Phys. **21**, 541 (1949).
[28] M. L. Plumer and M. B. Walker, J. Phys. C: Solid State Phys. **15**, 7181 (1982).
[29] E. Franus-Muir, M. L. Plumer, and E. Fawcett, J. Phys. C: Solid State Phys. **17**, 1107 (1984).
[30] A. E. Petrova and S. M. Stishov, J. Phys.: Condens. Matter **21**, 196001 (2009).
[31] A. B. Butenko, A. A. Leonov, U. K. Rößler, and A. N. Bogdanov, Phys. Rev. B **82**, 052403 (2010).
[32] A. A. Tereshchenko, A. S. Ovchinnikov, I. Proskurin, E. V. Sinitsyn, and J.-i. Kishine, Phys. Rev. B **97**, 184303 (2018).
[33] Y. Hu and B. Wang, New J. Phys. **19**, 123002 (2017).
[34] J. Wang, Y. Shi, and M. Kamlah, Phys. Rev. B **97**, 024429 (2018).
[35] T. L. Gilbert, IEEE Trans. Magn. **40**, 3443 (2004).
[36] P.-W. Ma, C. H. Woo, and S. L. Dudarev, Phys. Rev. B **78**, 024434 (2008).
[37] H. Wang, P.-W. Ma, and C. H. Woo, Phys. Rev. B **82**, 144304 (2010).
[38] H. Wen and C. H. Woo, Phys. Rev. E **94**, 032104 (2016).
[39] H. Wen and C. H. Woo, J. Nucl. Mater. **470**, 102 (2016).
[40] S. Guo, J. Wang, H. Du, C. Lu, C. Zhang, and Z. Lu, Comput. Mater. Sci. **142**, 285 (2018).
[41] C. H. Woo, H. Wen, A. A. Semenov, S. L. Dudarev, and P.-W. Ma, Phys. Rev. B **91**, 104306 (2015).
[42] A. E. Petrova, V. N. Krasnorussky, A. A. Shikov, W. M. Yuhasz, T. A. Lograsso, J. C. Lashley, and S. M. Stishov, Phys. Rev. B **82**, 155124 (2010).
[43] V. V. Brazhkin, L. N. Dzhavadov, and F. S. El'kin, JETP Lett. **104**, 99 (2016).
[44] S. V. Grigoriev, S. V. Maleyev, A. I. Okorokov, Y. O. Chetverikov, and H. Eckerlebe, Phys. Rev. B **73**, 224440 (2006).
[45] J. Chen, W. P. Cai, M. H. Qin, S. Dong, X. Lu, X. S. Gao, and J.-M. Liu, Sci. Rep. **7**, 7392 (2017).
[46] L. Verlet, Phys. Rev. **159**, 98 (1967).
[47] M. J. Uline and D. S. Corti, Entropy **15**, 3941 (2013).
[48] Y. Le Bras and J.-M. Greneche, Magneto-elastic resonance: Principles, modeling and applications, in *Resonance*, edited by J. Awrejcewicz (IntechOpen, London Bridge Street, 2017).
[49] Y. Nii, A. Kikkawa, Y. Taguchi, Y. Tokura, and Y. Iwasa, Phys. Rev. Lett. **113**, 267203 (2014).
[50] See Supplemental Material at http://link.aps.org/supplemental/10.1103/PhysRevB.100.144310 for analytical derivation of anisotropic elasticity feature of skyrmion materials.
[51] M. J. Buehler, *Atomistic Modeling of Materials Failure* (Springer Science & Business Media, Springer US, 2008).
[52] D. A. McQuarrie, *Statistical Thermodynamics* (Harper & Row, New York, 1973).
[53] H. Wen, J. Liu, Y. Wu, K. Lai, and Y. Zheng, arXiv:1811.07559.
[54] S. Stishov, A. Petrova, S. Khasanov, G. K. Panova, A. Shikov, J. Lashley, D. Wu, and T. Lograsso, J. Exp. Theor. Phys. **106**, 888 (2008).